The molecular basis for immune dysregulation by the hyperactivated E62K mutant of the GTPase RAC2

Received for publication, February 4, 2020, and in revised form, July 2, 2020 Published, Papers in Press, July 7, 2020, DOI 10.1074/jbc.RA120.012915

Megan E. Arrington[1], Brenda Temple[2,3], Antje Schaefer[4,5], and Sharon L. Campbell[2,5,*]

From the [1]Department of Chemistry, the [2]Department of Biochemistry and Biophysics, the [3]R. L. Juliano Structural Bioinformatics Core Facility, the [4]Department of Pharmacology, and the [5]Lineberger Comprehensive Cancer Center, University of North Carolina, Chapel Hill, North Carolina, USA

Edited by Alex Toker

The RAS-related C3 botulinum toxin substrate 2 (RAC2) is a member of the RHO subclass of RAS superfamily GTPases required for proper immune function. An activating mutation in a key switch II region of RAC2 ($RAC2^{E62K}$) involved in recognizing modulatory factors and effectors has been identified in patients with common variable immune deficiency. To better understand how the mutation dysregulates RAC2 function, we evaluated the structure and stability, guanine nucleotide exchange factor (GEF) and GTPase-activating protein (GAP) activity, and effector binding of $RAC2^{E62K}$. Our findings indicate the E62K mutation does not alter RAC2 structure or stability. However, it does alter GEF specificity, as $RAC2^{E62K}$ is activated by the DOCK GEF, DOCK2, but not by the Dbl homology GEF, TIAM1, both of which activate the parent protein. Our previous data further showed that the E62K mutation impairs GAP activity for $RAC2^{E62K}$. As this disease mutation is also found in RAS GTPases, we assessed GAP-stimulated GTP hydrolysis for KRAS and observed a similar impairment, suggesting that the mutation plays a conserved role in GAP activation. We also investigated whether the E62K mutation alters effector binding, as activated RAC2 binds effectors to transmit signaling through effector pathways. We find that $RAC2^{E62K}$ retains binding to an NADPH oxidase (NOX2) subunit, $p67^{phox}$, and to the RAC-binding domain of p21-activated kinase, consistent with our earlier findings. Taken together, our findings indicate that the $RAC2^{E62K}$ mutation promotes immune dysfunction by promoting RAC2 hyperactivation, altering GEF specificity, and impairing GAP function yet retaining key effector interactions.

RAC2 is a 21-kDa RAS superfamily GTPase that cycles between inactive GDP- and active GTP-bound states to regulate hematopoietic cell signaling in the immune system (1–3). In the most abundant white blood cell type, neutrophils, RAC2 regulates chemotaxis, phagocytosis, superoxide production, and actin polymerization (1, 4, 5). RAC2 is essential for proper immune function, and mutation of RAC2 leads to immune deficiencies (2, 6). Recently, a $RAC2^{E62K}$ mutant was identified in common variable immune deficiency (CVID). This hyperactivating mutation causes recurrent lung infections in patients and in $RAC2^{E62K/+}$ mice (2). Neutrophils from $RAC2^{E62K/+}$ CVID patients and mice showed enhanced macropinocytosis and superoxide production yet reduced chemotaxis (2). Given that the E62K mutation results in up-regulation of some RAC2-mediated processes and down-regulation of others, the mechanism of $RAC2^{E62K}$ dysregulation is likely complex.

RAC2 activation and cell signaling are controlled by the binding of regulatory factors and effector proteins, which associate with RAC2 via two highly dynamic regions termed "switch I" (Tyr^{32}–Asp^{38}) and "switch II" (Ala^{59}–Leu^{67}) (3). These regions rapidly "switch" between an open GDP-bound inactive conformation and a closed GTP-bound active conformation. Switching between the GTP- and GDP-bound states is controlled by the exchange of GDP for GTP and GTP hydrolysis, both intrinsically slow processes (3). Guanine nucleotide exchange factors (GEFs) stimulate GDP dissociation to up-regulate RAC2, whereas GTPase-activating proteins (GAPs) down-regulate RAC2 by stimulating GTP hydrolysis (7, 8). Guanine nucleotide dissociation inhibitors (GDIs) also down-regulate RAC2 by preventing association with the plasma membrane (7). Activated RAC2-GTP can bind downstream effectors such as $p67^{phox}$, which regulates superoxide production (9), and p21-activated kinases (PAKs), which regulate actin cytoskeleton organization (10), gene expression, and cell growth (11).

The $RAC2^{E62K}$ mutation is located directly within switch II, which engages GAPs as well as a subset of GEFs and effectors (12). Disease-causing mutations in RAC GTPases are rare and include the activating $RAC1^{P29S}$ mutant in melanoma (13) and the inactivating $RAC2^{D57N}$ mutant identified in CVID (6). These mutations directly perturb intrinsic guanine nucleotide binding yet do not affect GTP hydrolysis. The Glu^{62} residue is well-conserved across the RAS GTPase superfamily (in 100 of 141 family members) (14) and is adjacent to Gln^{61}, which plays a key role in catalyzing GTP hydrolysis (15). We previously determined that the E62K mutation does not affect intrinsic GTP hydrolysis but is defective in p50 RHOGAP–catalyzed GTP hydrolysis (2). Whereas Glu^{62} lies at the GAP-binding interface, it is unclear whether it plays a role in GAP-mediated hydrolysis. The RAS E62K mutation is impaired in p120 RASGAP–mediated GTP hydrolysis and promotes RAS activation (16), consistent with the identification of this mutant in malignant melanoma (17–19). Similarly, the GAP defect in $RAC2^{E62K}$ likely accounts for hyperactivation of $RAC2^{E62K}$ in $RAC2^{E62K/+}$ neutrophils and increased GTP loading observed in COS cells (2).

Whereas RAC2 is defective in p50 RHOGAP-mediated GTP hydrolysis, $RAC2^{E62K}$ GDP dissociation is not stimulated by the

This article contains supporting information.

* For correspondence: Sharon L. Campbell, campbesl@med.unc.edu.

addition of the Dbl homology (DH) GEF domain of TIAM1 (2). Intrinsic GDP dissociation rates for RAC2^{E62K} were unaffected, suggesting that the mutation does not directly affect nucleotide binding. Glutamate 62 likely modulates GEF activity in multiple GTPases (14, 15), as substitutions in RAS and RHOA to E62A or E62K inhibited GEF activity for CDC25 GEFs (RASGEFs) and DH domain RHOGEFs, respectively (14). Given these observations, it is unclear whether TIAM1 (and other DH domain GEFs) contributes significantly to RAC2^{E62K} nucleotide dissociation and activation in cells. RAC GTPases can also be activated by dedicator of cytokinesis (DOCK) GEFs, which bind RAC and CDC42 GTPases via switch I instead of switch II. Known RAC2 GEFs include the DH domain GEFS, TIAM1/2, VAV, and PREX1, and the DOCK domain GEFS, DOCK2 and DOCK5 (20–22). These GEFs not only activate RAC2, but also help direct RAC2-mediated signaling through their additional role as scaffolding proteins (20, 21). Hence, the severity of the RAC2^{E62K} GEF defect will not only affect GEF-mediated RAC2 activation but may alter localization with other RAC2-binding proteins that modulate downstream signaling.

The RAC2^{E62K} hyperactivating mutation is a monogenic cause of CVID (2). We recently determined that RAC2^{E62K} retains intrinsic biochemical properties but exhibits defects in TIAM1 and p50 RHOGAP activity (2). To understand why these defects exist and to predict other potentially affected protein-protein interactions, we sought to more comprehensively characterize the RAC2^{E62K} CVID mutant. Whereas CD analysis and molecular dynamics simulations indicate that the E62K mutation does not significantly alter RAC2 stability and structure, the E62K mutation impairs GAP activity for multiple GTPases (2). We find that KRAS^{E62K} is defective in p120 RASGAP–stimulated GTP hydrolysis, suggesting a conserved role of Glu^{62} in both GEF and GAP interactions. In a more thorough study of RAC2^{E62K} TIAM1 GEF–stimulated dissociation herein, RAC2^{E62K} is completely insensitive to TIAM1 stimulation, indicating that TIAM1, and likely other DH domain GEFs, do not significantly contribute to RAC2^{E62K} activation. Notably, whereas the E62K mutation ablates TIAM1 activity, DOCK2 activity is retained. These findings highlight a potential shift in RAC2 GEF specificity. Finally, we find that the E62K mutation retains binding to the effector proteins p67^{phox} and PAK, consistent with observations that RAC2^{E62K} promotes superoxide production and the actin cytoskeleton network in cells (2). Our findings suggest that the changes in RAC2^{E62K}-mediated cell signaling may be driven by altered interactions with regulatory proteins. Results from this study not only highlight possible molecular mechanisms for RAC2-driven CVID but also outline a critical role for Glu^{62} in GTPase regulation.

Results

RAC2^{E62K} retains similar secondary structure and stability to RAC2^{WT}

In RAS superfamily GTPases, Glu^{62} is positioned within the highly dynamic switch II region. Given its position adjacent to Gly^{60} and Gln^{61}, which are essential for GTP hydrolysis (3, 15), structural perturbations at Glu^{62} could perturb GTPase activity as well as RAC2 structure and stability. However, existing crystal structures for RAC1^{WT}, RAC1^{Q61L}, and RAC2^{G12V} suggest that Glu^{62} is solvent-exposed and does not form intramolecular contacts or interact with the guanine nucleotide in either the inactive GDP-bound or active GTP analog (GMPPNP)-bound states (23–26). To determine whether the E62K mutation alters the structure and stability of RAC2, we performed biophysical studies of RAC2^{E62K} in its active and inactive conformations.

To assess protein secondary structure and stability, we conducted CD analyses on RAC2^{WT} and RAC2^{E62K} in both the inactive GDP-bound state and the active GTP-bound conformation at 20 °C in the far-UV region (200–250 nm) (27). The GTP-bound state was maintained by loading RAC2 with the nonhydrolyzable GTP analog GMPPCP. As shown in Fig. 1 (*A* and *B*), no significant change in the CD spectrum was observed for the mutant in either the GDP- or GMPPCP-bound state, respectively. Additionally, the profile of the CD scans is similar to those observed for other RAC and RAS GTPases (28, 29), indicating that RAC2^{WT} and RAC2^{E62K} exhibit the secondary structure and fold of other closely related small GTPases.

To access protein stability, thermal denaturation scans were conducted at 222 nm over a temperature range from 20 to 95 °C. The melting temperatures of GDP-bound (Fig. 1*C*) RAC2^{WT} and RAC2^{E62K} were 55 and 54 °C respectively, whereas the GMPPCP-bound (Fig. 1*D*) melting temperatures were slightly lower at 52 °C (Table S1). The minimal changes observed in the thermal melting temperature indicate that RAC2 is stably folded in both nucleotide (GDP, GTP)-bound states. Additionally, similar cooperativity of the denaturation curves is observed, indicating that both proteins unfold in a similar manner. Taken together, these results indicate that the E62K mutation does not significantly alter RAC2 structure or stability. CD can also indirectly detect changes in guanine nucleotide binding, as RAC GTPases are stabilized by multiple interactions with guanine nucleotide ligands. A decrease in guanine nucleotide binding, such as that observed for RAC1^{P29S} (25) and glutathiolated RAC1 (28), results in a decrease in protein stability and is reflected by a decreased thermal denaturation temperature (T_m). The similar melting temperatures observed for RAC2^{WT} and RAC2^{E62K} support retention of nucleotide binding, consistent with our previous findings that RAC2^{E62K}-GDP dissociation rates are similar to those for RAC2^{WT} (2).

Molecular dynamics simulations predict that the E62K mutation does not significantly alter the three-dimensional structure of RAC2

To further assess whether the E62K mutation alters the conformation and dynamics properties of RAC2^{E62K} in both the active-GTP and inactive-GDP bound states, we ran 750-ns molecular dynamics simulations for both WT RAC2 and RAC2^{E62K} in the GDP- and GTP-bound states. As a crystal structure of RAC2^{WT} in either the GDP- or GTP-bound state is lacking, we first generated structural models of RAC2^{WT} and RAC2^{E62K} bound to GDP and GTP from the existing crystal structures of RAC2^{G12V}-GDP (26) and RAC1^{WT}-GMPPNP (23), respectively, and performed AMBER molecular dynamics simulations in triplicate, for a total of 12 simulations. Calculations of structural fluctuations, time-averaged

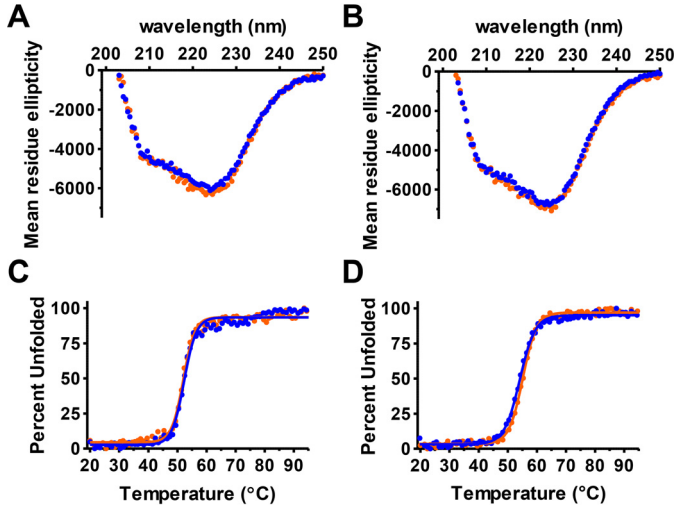

Figure 1. RAC2^{E62K} retains secondary structure and thermal stability. *A* and *B*, CD spectral overlay of RAC2^{WT} (*orange*) and RAC2^{E62K} (*blue*) bound to GDP (*A*) and GMPPCP (*B*). Scans were collected at 20 °C from 200 to 250 nm. Mean residue ellipticity was calculated as described previously (27, 28). Thermal unfolding was measured by CD (222 nm) over a temperature range of 20–95 °C for 5 μM GDP-bound RAC2^{WT} and RAC2^{E62K} (*C*) and GMPPCP-bound RAC2^{WT} and RAC2^{E62K} (*D*). Thermal unfolding was quantified by the loss of mean residue ellipticity at 222 nm and normalized relative to the maximum and minimum ellipticity. Thermal denaturation curves and T_m were calculated by fitting the thermal denaturation data (*C* and *D*) to a Boltzmann sigmoidal curve using GraphPad Prism. Plots are representative of three independent experiments. Thermal denaturation curves are representative of triplicate and duplicate experiments for GDP- and GMPPCP-bound RAC2, respectively.

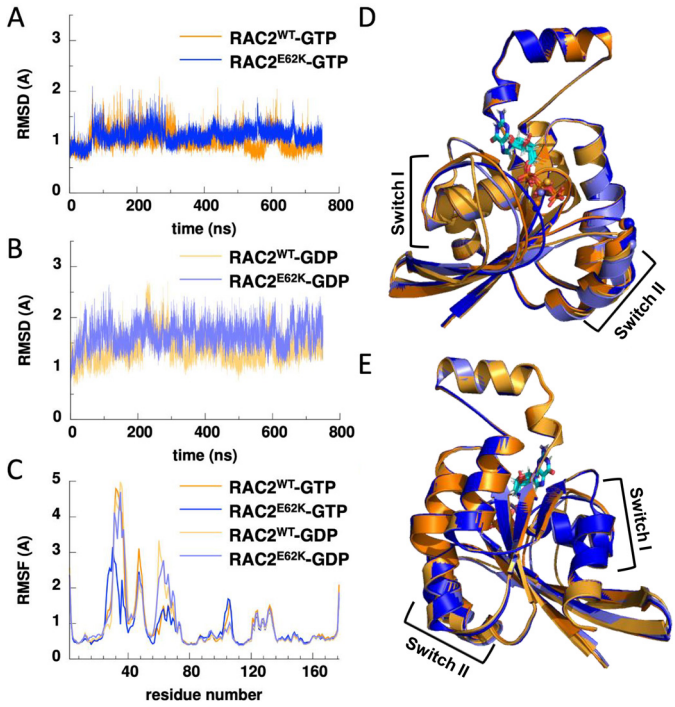

Figure 2. Molecular dynamic simulations predict that the E62K mutation does not significantly alter the RAC2 structure. Representative trajectories from MD simulations of GTP-bound (*A*) and GDP-bound (*B*) RAC2^{WT} and RAC2^{E62K} show that equilibrium was achieved within 750 ns. GTP-bound RAC2^{E62K} shows smaller RMSD fluctuations (*C*) about the average structure relative to GTP-bound RAC2^{WT}, as calculated from the combined trajectories of three independent MD simulations over 100–750 ns. Variability between RAC2^{WT} and RAC2^{E62K} is localized to the dynamic switch I region. *D* and *E*, overlay of average structures from three independent 750-ns MD simulations for RAC2^{WT} (in *orange*) and RAC2^{E62K} (in *blue*) in both the GTP-bound (*darker shades*) and GDP-bound forms (*lighter shades*). Switch I and switch II are in the foreground (in *D*) and the background (in *E*) and are indicated in *brackets*. Starting structural models for RAC2 bound to GDP and GTP were generated from the crystal structures of RAC2^{G12V}-GDP (PDB entry 2W2T) (27) and RAC1^{WT}-GMPPCP (PDB entry 1MH1) (24), respectively. Data representing RAC2^{WT} and RAC2^{E62K} simulations are *colored* in *orange* and *blue*, respectively. The Glu^{62} C-α is shown as a *sphere* in *orange* and *blue* for RAC2^{WT} and RAC2^{E62K}, respectively. The cofactor Mg^{2+} is indicated as a *sphere*, and the bound nucleotide is *colored* by element.

structures, and density peaks clustering analyses (30) were completed.

We first calculated the root mean square deviation (RMSD) in the positions of the Cα atoms for residues 4–24 and 43–177 (omitting the dynamic switch I), by comparing with the starting structural models. Representative trajectories for each of the four conformations are plotted in Fig. 2 (*A* and *B*), clearly showing that the simulations have equilibrated by 100 ns. We then calculated average RMSDs, along with average structures, over all snapshots in the trajectories of the three replicates. The RMSDs serve as one measure of the variation in the RAC2 conformational ensemble. Simulations of the GTP-bound conformations had mean RMSDs of 1.16 ± 0.24 and 1.12 ± 0.20 Å for RAC2^{WT} and RAC2^{E62K}, respectively. Simulations of the GDP-bound conformations had RMSDs of 1.37 ± 0.27 and 1.45 ± 0.29 Å for RAC2^{WT} and RAC2^{E62K}, respectively.

Fluctuations about average structures serve as a second measure of variation in the conformational ensemble and were calculated over the range of 100–750 ns for the combined trajectories (Fig. 2*C*). Root-mean-square-fluctuations about the average structure for GTP- and GDP-bound conformations showed a constrained switch II in the GTP-bound conformation compared with the GDP-bound conformation, as expected due to the coordination of the γ-phosphate of GTP. Importantly, there were no significant differences in fluctuations of switch II, which contains the E62K mutation, between RAC2^{WT} and RAC2^{E62K} in either the GDP- or GTP-bound conformations.

The average structures of the combined trajectories capture the dynamic motions in switches I and II, as shown in Fig. 2 (*D* and *E*), and do not show significant differences outside switch I and II, for either the GDP- or GTP-bound conformations over 100–750 ns. In the GTP-bound state, the average structures show slight differences in the conformation of switch I, which has been reported to be more dynamic in RAC2 GTPases compared with the other RAC isoforms (31). We performed a density peaks–based clustering analysis (30) on the combined trajectories to identify clusters of conformations within each trajectory. For RAC2^{WT}-GTP, two clusters were identified, one containing 77.6% of the snapshots and the other with 22.4% of the snapshots (Fig. S1*A*), with the smaller cluster showing a more open conformation for switch I. A single cluster containing 100.0% of the snapshots was identified within the trajectory from the RAC2^{E62K} GTP-bound simulations (Fig. S1*B*). These snapshots are similar to those observed in the larger cluster for GTP-bound RAC2^{WT}. Together, these results show that the E62K mutation does not alter RAC2 structure but may induce

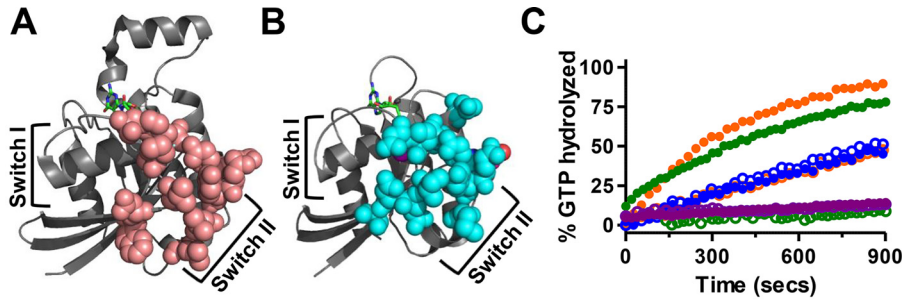

Figure 3. The E62K mutation in both RAC2 and KRAS perturbs GAP-stimulated GTP hydrolysis. Glutamate 62 is highly conserved in RAS superfamily GTPases and lies at the GAP interface in structures of multiple GTPase/GAP complexes. *A*, *ribbon diagram* of the $RAC1^{WT}$ crystal structure (PDB entry 1HE1) bound to the GAP domain of ExoS (not shown) generated in PyMOL, highlighting the RHOGAP-binding site (*salmon*) (38). *B*, *ribbon diagram* of the $HRAS^{WT}$ crystal structure (PDB entry 1WQ1) bound to the GAP domain of p120 RASGAP (not shown) generated in PyMOL highlighting the RASGAP-binding site (*cyan*) (37). Glutamate 62 lies in proximity to the binding interface and is *color-coded* by atom. Residues within 5 Å of ExoS or p120 RASGAP are shown in *salmon* and *cyan*, respectively, as calculated using the Protein Interactions Calculator web server (73). The cofactor Mg^{2+} is indicated as a *sphere*, and the bound nucleotide (GDP and AlF_3 to mimic GTP) is *colored* by element. *C*, single-turnover intrinsic (*open circles*) and GAP-stimulated (*closed circles*) GTP hydrolysis curves for $KRAS^{WT}$ (*green*) and $KRAS^{E62K}$ (*purple*) as measured by the detection of P_i using FLIPPi 5U. Intrinsic and p50 RHOGAP-stimulated GTP hydrolysis curves for $RAC2^{WT}$ (*orange*) and $RAC2^{E62K}$ (*blue*) are shown for comparison as reported previously (2). These data were compared with our findings on the $KRAS^{E62K}$ mutant to highlight the similar trends in GTP hydrolysis for both mutants. KRAS (5 μM) was preloaded with GTP and hydrolysis of GTP initiated by the addition of 1 mM $MgCl_2$ in the absence (*open circles*) and presence (*closed circles*) of the p120 RASGAP (25 nM) catalytic GAP domain, as described previously for RAC2 (2). GTP hydrolysis rates were calculated by fitting single-phase association curves using GraphPad Prism. Curves are representative of two independent experiments each, collected in duplicate. GTP hydrolysis rates are reported as mean ± S.D. in Table S2.

minor perturbations localized to switch I in the active GTP-bound state.

In the inactive GDP-bound state, two clusters were identified for both the WT and mutant proteins in the snapshots from the respective trajectories. $RAC2^{WT}$ had one cluster containing 66.8% of the snapshots with the remaining cluster containing 33.2% (Fig. S1*C*). $RAC2^{E62K}$ had a similar distribution between the two clusters, with 66.7% of the snapshots in the largest cluster and 33.3% of the snapshots in the smaller cluster (Fig. S1*D*). For the GDP-bound conformations, most of the variability between clusters also lies within switch I. However, the variability is consistent between $RAC2^{WT}$ and $RAC2^{E62K}$. In summary, the RAC2 E62K mutation does not appear to alter the RAC2-GDP structure. Moreover, only minor changes in the dynamic switch I regions are observed for the RAC2-GTP structure. These results are consistent with CD analysis of protein secondary structure and thermal stability. Together, these results suggest that that the E62K mutation does not significantly alter the three-dimensional structure of RAC2 in either the GDP- or GTP-bound state.

The E62K mutation impairs GAP activity in both RAC2 and KRAS

$RAC2^{E62K}$ is an activating mutation that increases RAC2 GTP activation and alters RAC2-mediated cellular phenotypes in neutrophils (2). Hyperactivation of RAC2 by the E62K mutation is likely driven by the p50 RHOGAP defect, as intrinsic GTP hydrolysis is unaffected (2). Whereas Glu^{62} does not appear to contribute to intrinsic GTP hydrolysis, it lies directly within the GAP-binding interface in multiple RAS superfamily GTPases (32–34) and may disrupt GAP association with other RAS-related GTPases. The GAP-binding interfaces of RAC1 (Fig. 3*A*) and HRAS (Fig. 3*B*) with the RHOGAP EXOS (35) and p120 RASGAP (34), respectively, are highlighted to illustrate the location of Glu^{62} within the GAP-binding interface.

To examine whether the E62K mutation disrupts GAP activity for multiple GTPases, we measured the intrinsic and p120 RASGAP-stimulated GTP hydrolysis rates for $KRAS^{WT}$ and $KRAS^{E62K}$ (both in Fig. 3*C*) and compared these activities with those previously observed by us for RAC2 (2). We selected RAS because Glu^{62} mutations have been identified in human cancers for all RAS isoforms (KRAS, HRAS, and NRAS) (16–19, 36). To measure KRAS GTP hydrolysis activity, we monitored the production of P_i using the phosphate-binding protein, FLIPPi 5U, as described previously (37, 38). To measure single-turnover hydrolysis rates, $KRAS^{WT}$ and $KRAS^{E62K}$ protein were preloaded with GTP, and hydrolysis was initiated by the addition of $MgCl_2$ without and with the catalytic GAP domain (GAP-334) of p120 RASGAP (1:200 GAP/RAS). Consistent with previous findings for $KRAS^{WT}$ (29, 39), p120 RASGAP stimulates $KRAS^{WT}$ GTP hydrolysis ~7-fold (Fig. 3*C*) relative to the intrinsic rate (Table S2).

Similar to $RAC2^{E62K}$, the RAS E62K mutation does not significantly perturb intrinsic GTP hydrolysis compared with $KRAS^{WT}$ but is defective in GAP-mediated GTP hydrolysis (1:200 p120 RASGAP catalytic domain/RAS). The observed $KRAS^{E62K}$ GAP defect may cause KRAS hyperactivation and may drive deregulated growth control in cancer patients with this mutation (16–19). To compare the effects of the E62K mutation between RAC2 and KRAS on GTP hydrolysis, we overlay our previously reported results for RAC2 (2) with the results for KRAS. As shown in Fig. 3*C*, the E62K mutation does not perturb intrinsic GTP hydrolysis but induces a GAP defect in both RAS and RAC2 GTPases. This is a valid comparison because the data were collected using the same methods (2). Hence, these findings support a conserved role of Glu^{62} in GAP-stimulated GTP hydrolysis and provide evidence that the E62K mutation can induce hyperactivation in multiple GTPases.

$RAC2^{E62K}$ is insensitive to DH RAC GEF TIAM1 regulation

Previously, we determined that $RAC2^{E62K}$ GDP dissociation is not stimulated by the catalytic DH GEF domain of TIAM1 (2). Because $RAC2^{E62K}$ intrinsic GDP dissociation was not

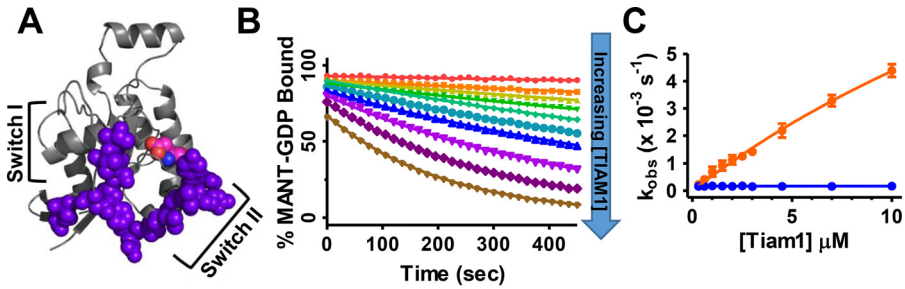

Figure 4. RAC2^{E62K} retains intrinsic nucleotide binding but is defective in TIAM1 GEF-stimulated GDP dissociation. The Glu^{62} residue lies adjacent to the TIAM1-binding interface. *A*, *ribbon diagram* generated in PyMOL of nucleotide-free RAC1^{WT} (PDB entry 1FOE) bound to TIAM1 (not shown), highlighting the TIAM1-binding site (43). Glutamate 62 lies in proximity to the binding interface and is *color-coded* by atom. Residues within 5 Å of TIAM1 (*purple*) are highlighted as calculated using the Protein Interactions Calculator web server (73). *B*, intrinsic and GEF-stimulated MANT-GDP dissociation curves for RAC2^{WT}. RAC2 was preloaded with MANT-GDP, and dissociation was initiated by the addition of 1000-fold excess GDP in the absence and presence of varying GEF concentrations. TIAM1 concentration is indicated as follows: intrinsic dissociation (0 μM TIAM1, in *red*) and increasing TIAM1 concentration (0.3 μM (*orange*) to 10 μM (*brown*)). Nucleotide dissociation rates were calculated by fitting curves with a single-phase exponential decay using GraphPad Prism. Curves are representative of three independent experiments. *C*, nucleotide dissociation rates for RAC2^{WT} (in *orange*) and RAC2^{E62K} (in *blue*) plotted as a function of TIAM1 concentration to assess changes in TIAM1 catalytic activity. RAC2 concentrations were constant at 3 μM, and TIAM1 concentrations were varied from to 0.3 to 10 μM. MANT-GDP dissociation rates are reported as mean ± S.D. as calculated in GraphPad Prism for three independent experiments.

perturbed, the TIAM1 GEF defect is likely due to a decrease in TIAM1 binding. Multiple crystal structures show that the Glu^{62} residue lies at the binding interface for multiple GEFs and GTPases, including in the crystal structures of RAC1^{WT} in complex with TIAM1 (40), HRAS with SOS (41), and RHOA with DBS (42). Indeed, Glu^{62} substitutions in both RHOA and KRAS cause defects in GEF-stimulated GDP dissociation (14). To illustrate the position of Glu^{62} within the TIAM1-binding interface, residues in RAC1 that are within 5 Å of TIAM1 are highlighted in Fig. 4*A*. TIAM1 is one of several DH domain GEFs that activate RAC2. Others include VAV1 and PREX1 GEFs, which also play a role in RAC2-mediated cell signaling in neutrophils (43, 44). We have focused on RAC2^{E62K} TIAM1-stimulated GDP dissociation because TIAM1 is highly specific for RAC2 (31). Additionally, the RAC-TIAM1–binding interface is well defined (40, 42), and we have previously used this TIAM1 construct to assess GEF-stimulated GDP dissociation *in vitro* (28, 45). Importantly, the DH domains in VAV1, PREX1, and TIAM1 are structurally conserved and bind to RAC1 at the same interface (40, 46, 47). Thus, our TIAM1 findings herein are likely predictive of other DH domain RAC2 GEFs.

Our previous finding that the TIAM1 GEF domain does not stimulate RAC2^{E62K} GDP dissociation indicates that the E62K mutation causes a GEF defect (2). However, because those studies were only completed at a single concentration (1:1 ratio RAC2/TIAM1), the extent of this defect was unclear because the catalytic efficiency was not assessed. To quantitatively assess how the E62K mutation affects TIAM1 activity, we conducted nucleotide dissociation assays to calculate the catalytic efficiency, k_{cat}/K_m, for TIAM1-stimulated GDP dissociation. To measure nucleotide dissociation rates *in vitro*, we preloaded RAC2 with fluorescent MANT-GDP and observed MANT-GDP dissociation upon the addition of excess GDP. The intrinsic GDP dissociation rates for RAC2^{WT} ($1.9 \pm 0.9 \times 10^{-4}$ s^{-1}) and RAC2^{E62K} ($2.1 \pm 0.3 \times 10^{-4}$ s^{-1}) are consistent with those reported previously (2). Representative nucleotide dissociation curves for RAC2^{WT} and RAC2^{E62K} are shown in Fig. 4*B* and Fig. S2*A*, respectively, with the rates quantified in Fig. 4*C*. As expected for RAC2^{WT}, the addition of the TIAM1 GEF domain increases GDP dissociation over the intrinsic rate. RAC2^{WT} GDP nucleotide dissociation is catalyzed by the addition of the TIAM1 GEF domain with a catalytic efficiency (k_{cat}/K_m) of 560 M^{-1} s^{-1} (Table S3). Importantly, RAC2^{E62K} GDP dissociation was not stimulated by TIAM1 at even 5-fold excess TIAM1/RAC2, indicating that the E62K mutation completely abolishes TIAM1 stimulation of GDP dissociation. This complete loss in TIAM1 catalytic activity strongly suggests that TIAM1 (and likely other DH domain GEFs) does not contribute to RAC2^{E62K} activation in cells.

RAC2^{E62K} is activated by the DOCK2 GEF

Whereas the Glu^{62} lies at the binding interface for DH domain GEFS, another class of RAC-GEFs exists. The DOCK-A subfamily GEFs (DOCK180, DOCK2, and DOCK5) bind to RAC GTPases at a distinct interface from DH domain GEFs. As shown in Fig. 5*A*, DOCK GEFs primarily engage RAC GTPases through switch I rather than switch II and activate RAC GTPases via a distinct mechanism (48, 49). Thus, we postulated that RAC2^{E62K} retains DOCK GEF-stimulated GDP dissociation. To test whether RAC2^{E62K} can be activated by DOCK A GEFs, we used the DOCK2 catalytic GEF domain to carry out GDP dissociation assays. We chose DOCK2, as this GEF is expressed selectively in hematopoietic cells and is required for superoxide production and macropinocytosis in neutrophils (4). Importantly, the DOCK homology region 2 (DHR2) catalytic GEF domain is highly conserved between the DOCK A GEFs and is representative of the ability of DOCK180, DOCK2, and DOCK5 to activate RAC2^{E62K}.

To determine whether the E62K mutation alters the catalytic activity of the DOCK2 DHR2 domain, we measured MANT-GDP dissociation rates at varying concentrations of DOCK2 for RAC2^{WT} and RAC2^{E62K}. Representative nucleotide dissociation curves are shown for RAC2^{WT} and RAC2^{E62K} in Fig. S2*B* and Fig. 5*B*, respectively, with nucleotide dissociation rates quantified in Fig. 5*C*. Importantly, the DOCK2 GEF domain stimulated GDP dissociation for both RAC2^{WT} and RAC2^{E62K} with catalytic efficiencies (k_{cat}/K_m) of 3100 M^{-1} s^{-1} and 4100 M^{-1} s^{-1}, respectively. The k_{cat} and K_m values reported in Table

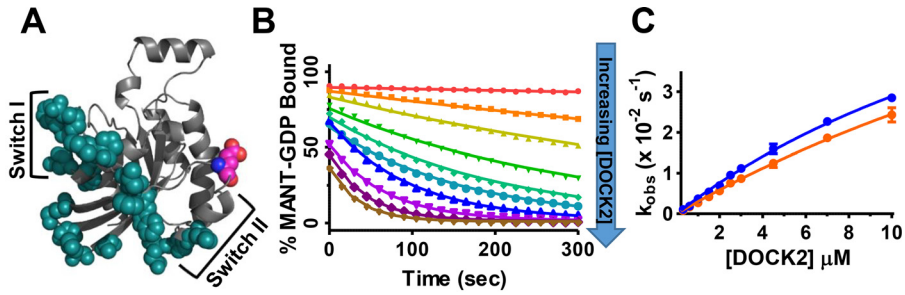

Figure 5. RAC2^{E62K} retains DOCK2-stimulated nucleotide exchange. The DOCK2 DHR2 GEF domain binds a distinct region of RAC from DH GEFs. *A*, *ribbon diagram* of nucleotide-free RAC1^{WT} (PDB entry 2YIN) bound to DOCK2 (not shown) (51), highlighting the DOCK2-binding site. Glutamate 62 lies outside of the DOCK2-binding interface and is *color-coded* by atom. Residues within 5 Å of DOCK2 are shown in *teal* and were calculated using the Protein Interactions Calculator web server (73). *B*, intrinsic and GEF-stimulated MANT-GDP dissociation curves for RAC2^{E62K}. RAC2 was preloaded with fluorescent MANT-GDP, and dissociation was initiated by the addition of 1000-fold excess GDP and varying concentrations of the DOCK2 DHR2 GEF domain. DOCK2 concentration is indicated as follows: intrinsic dissociation (0 μM, in *red*) and increasing DOCK2 concentration (0.3 μM (*orange*) to 10 μM (*brown*)). Nucleotide dissociation rates were calculated by fitting curves with a single-phase exponential decay in GraphPad Prism. Curves are representative of three independent experiments. *C*, nucleotide dissociation rates were plotted as a function of DOCK2 concentration to assess changes in DOCK2 catalytic activity. RAC2 concentrations were constant at 3 μM, and DOCK2 concentrations were varied from 0.3 to 10 μM. Nucleotide dissociation rates are reported as mean ± S.D. for three independent experiments.

S3 show that this modest difference in DOCK2 catalytic efficiency is not significant. These findings indicate that RAC2^{E62K} retains DOCK2 catalytic activity relative to RAC2^{WT}. Given the direct correlation between GEF binding and activity, the E62K mutation also does not perturb RAC2-DOCK2 binding. Our results for TIAM1- and DOCK2-stimulated GDP dissociation together suggest that the E62K mutation alters GEF specificity so that DOCK GEFs, but not DH-RAC GEFs, activate RAC2^{E62K} in cells.

RAC2^{E62K} binds the effectors p67^{phox} and PAK

Once activated, RAC2-GTP binds effectors to direct cell signaling downstream; thus, any perturbations in effector binding will dysregulate RAC2-mediated cell signaling. In neutrophils, RAC2 activates NADPH oxidase (NOX2) by binding p67^{phox}, the cytosolic catalytic subunit of the NOX2 complex. Upon RAC2-p67^{phox} binding, a conformational change occurs in NOX2 that drives electron transport across the membrane to molecular oxygen producing superoxide (50). As the RAC2^{E62K} mutant displays increased and sustained production of superoxide in CVID patient neutrophils and in mice (2), we anticipated that the mutant would retain p67^{phox} binding. The RAC-binding domain (RBD) of p67^{phox} binds RAC via switch I, as shown in Fig. 6*A*, and the binding interface is far away from the E62K mutation site.

To measure p67^{phox} binding to RAC2^{WT} and RAC2^{E62K}, we employed isothermal titration calorimetry (ITC), as this method not only provides stoichiometry and binding affinity, but also thermodynamics associated with binding. The heat absorbed upon binding of p67^{phox}-RBD to GMPPCP-loaded RAC2^{WT} and RAC2^{E62K} is shown (Fig. 6*B*) along with the binding isotherms associated with titration of p67^{phox} with GMPPCP-bound RAC2^{WT} and RAC2^{E62K}. Binding affinities, stoichiometry, and heats of binding are listed in Table S4. Binding was approximately stoichiometric ($n \sim 0.8$-0.9) with equilibrium dissociation constants (K_D = 2.6 and 1.8 μM for RAC2^{WT} and RAC2^{E62K}, respectively) similar to that reported previously for RAC2^{Q61L} (51). The results indicate that RAC2^{E62K} binds to p67^{phox} with similar affinity as RAC2^{WT}, consistent with enhanced superoxide levels observed for this mutant in RAC2$^{E62K/+}$ patient neutrophils and COS cells (2).

RAC2 also regulates multiple cell-signaling pathways through the activation of PAKs, which in turn activate multiple targets, including LIM kinase (52), p47^{phox} (53), and RAF1 (RAF proto-oncogene serine/threonine kinase) (54). Additionally, the PAK-binding assay is an important tool for measuring RAC activation in cells, including the RAC activation assay reported in our previous work (2). A change in RAC2-PAK binding would lead to errors in assessing cellular RAC activity using PAK pulldown approaches. Using this assay, we recently observed increased RAC2^{E62K} activation in COS cells, indicating a retention of PAK binding (2). To assess whether the E62K mutant retains PAK-RBD binding similar to RAC2^{WT}, we conducted ITC experiments with GMPPCP-loaded RAC2. As shown in Fig. 6*C*, we find that RAC2^{E62K} binds PAK with a similar affinity as RAC2^{WT}. The binding affinities, stoichiometry, and heat upon binding are reported in Table S3. RAC binding to the PAK-RBD is approximately stoichiometric (n = 0.78 and 0.88 for RAC2^{WT} and RAC2^{E62K}, respectively; Table S3).

PAK-RBD binding to RAC2 causes heat release (exothermic reaction) compared with the heat absorbed (endothermic reaction) associated with binding of RAC2 to p67^{phox}. This difference in binding energetics is most likely attributable to differences in binding interactions. As shown in Fig. 6*A*, the binding interfaces of RAC2 with the RBDs of PAK and p67^{phox} are quite distinct. The PAK-RBD engages RAC2 via β2 and switch 2 (55), whereas p67^{phox} binds primarily via switch I (51). Notably, RAC2^{E62K} retains both p67^{phox} and PAK-RBD binding even though the effectors bind at different sites (Fig. 6*A*). These findings are consistent with the structural model shown in Fig. 2*D*, indicating retention of RAC2^{E62K}-GTP structure. Given these results, we predict that only effectors or regulatory proteins that directly bind near the mutation site may be affected by this activating mutation.

Discussion

The RAC2 small GTPase is required for immune function (56, 57). Recently, it was shown that the RAC2$^{E62K/+}$ mutation directly causes CVID (2). Herein, we further characterize this

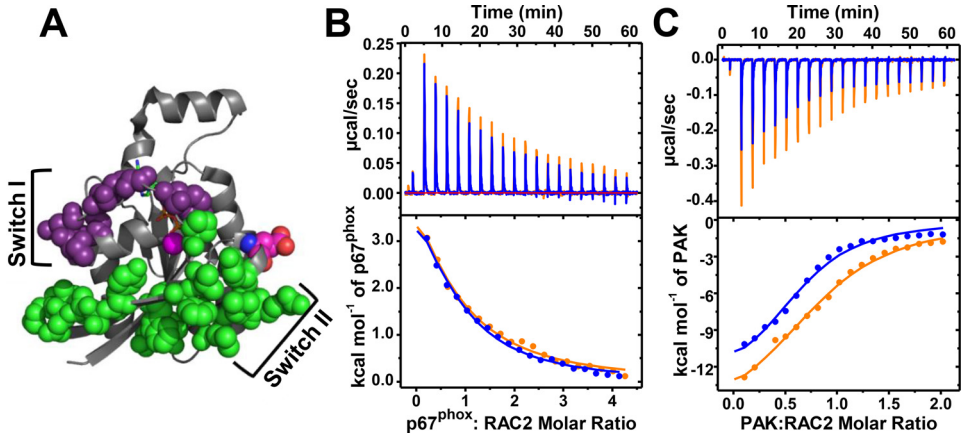

Figure 6. RAC2^{E62K} retains binding to the RAC-binding domains of p67^{phox} and PAK. The RAC RBDs of p67^{phox} and PAK bind to different sites on GTP-bound RAC Q61L. *A*, *ribbon diagram* of RAC1^{Q61L} generated in PyMOL. RAC residues that contact p67^{phox} and PAK-RBD mapped onto the GTP-bound RAC1^{Q61L} structure (PDB entry 1E96) as shown in *blue* and *green spheres*, respectively (53). The p67^{phox}-RBD contacts switch I and the $\beta5/\alpha5$ loop in RAC1^{WT} (53), whereas the PAK-RBD contacts switch II and $\beta2$ in CDC42 (57). Glutamate 62 is indicated as *spheres* and *colored* by atom. The nucleotide GTP is shown as *sticks colored* by atom, and the cofactor Mg^{2+} is shown as a *magenta sphere*. *B*, isothermogram of RAC2^{WT} and RAC2^{E62K} in the presence of varying concentrations of p67^{phox} RBD at 25 °C. The p67^{phox}-RBD (0–100 μM) was injected at 510 μM into a cell containing 25 μM GMPPCP-loaded RAC2. The data were processed and curve-fit using a single-site model in Origin 7.0. Data are representative of triplicate experiments. *C*, isothermogram for RAC2^{WT} (*orange*) and RAC2^{E62K} (*blue*) in the presence of varying concentrations of PAK-RBD at 25 °C. The PAK-RBD (0–30 μM) was injected at 150 μM into a cell containing 15 μM GMPPCP-loaded RAC2. Data were fit as in *A* and are representative of duplicate experiments. The heat absorbed (upon p67 binding) or released (upon PAK binding) was integrated per 2-μl injection over 20 injections using a microCal ITC 200 instrument. Binding stoichiometry (*n*), K_D, enthalpy, and entropy values were calculated using Origin 7.0. Values are reported as the mean ± S.D. in Table S3.

immune dysfunction mutant. Consistent with previous results showing retention of intrinsic GTP hydrolysis and GDP dissociation, we found that RAC2^{E62K} structure, fold, and stability were not significantly perturbed in either the active GMPPCP-bound or inactive GDP-bound state *in vitro* (Fig. 1). Further, molecular dynamics simulations and clustering analyses indicate that the E62K mutation does not significantly alter the RAC2 structure (Fig. 2 and Fig. S1). These results are consistent with the surface exposure and lack of intramolecular contacts associated with Glu^{62} in multiple crystal RAC structures (23, 24, 26).

Hyperactivation of RAC2^{E62K} previously observed in COS cells is likely driven by the observed p50 RHOGAP defect (2). RAC2, like other RHO GTPases, is down-regulated by both GAPs and RHOGDIs. Whereas GAPs inactivate by accelerating GTP hydrolysis, GDIs prevent activation by preventing membrane association (7). Because RAC2^{E62K} is hyperactivated in cells, it is unlikely that GDI binding is perturbed as this would down-regulate RAC2^{E62K} activity. The GAP defect observed for both KRAS^{E62K} and RAC^{E62K} (Fig. 3*C*) suggests that Glu^{62} plays a key role in GAP association and catalysis across the RAS superfamily GTPases. Crystal structures of CDC42 and RHOA in complex with the catalytic domain of p50 RHOGAP show a contact between Glu^{62} (Glu^{64}, RHOA numbering) and Arg^{346} in p50 RHOGAP (32, 58). Thus, in RAC2, Glu^{62} likely makes a similar contact with p50 RHOGAP, with the E62K mutation disrupting this key contact and thereby perturbing p50 RHOGAP-stimulated GTP hydrolysis. Similarly, the crystal structure of HRAS with p120 RASGAP shows a contact between Glu^{62} in HRAS and Arg^{749} in RASGAP (34) and provides insight into how this nonconservative charge-reversal mutation perturbs GAP binding. Our results herein suggest that Glu^{62}-GAP interactions facilitate GTP hydrolysis and that the E62K mutation causes a GAP defect that mediates RAC2 (and potentially RAS) up-regulation in cells.

The Glu^{62} residue plays a key role in GEF-stimulated GDP dissociation by DH domain GEFs. In crystal structures of GTPases with DH domain GEFs, Glu^{62} forms a salt bridge with Lys^{16} in the phosphoryl-binding loop (14, 15). In the structures of RAC1 in complex with the DH GEF domains of VAV1 (46), PREX1 (47), and TIAM1 (45), similar reorientation of Glu^{62} toward Lys^{16} is observed, supporting a key role of Glu^{62} in stabilizing the nucleotide-free from of RAC. Additionally, Gasper *et al.* (14) found that RHOA^{E64K} and KRAS^{E62K} substitutions abolish GEF-stimulated GDP dissociation by p115 RHOGEF (also known as ARHGEF1) and SOS, respectively. Based on these observations, we predict that the TIAM defect observed for RAC2^{E62K} (Fig. 4) will translate to other DH domain GEFs, including VAV, PREX, and TIAM2, as well as to other GTPases. Because RAC2^{E62K} DOCK2 activity is retained, DOCK2 likely compensates for the loss in DH domain GEF activity and contributes to RAC2^{E62K} in cells.

RAC2 is activated by the DOCK A GEFs (DOCK180/1, DOCK2, and DOCK5) (48), which disrupt GDP binding and stimulate nucleotide exchange by extending the conformation of switch I and displacing the cofactor Mg^{2+} (59). The DHR2 GEF domain of DOCK2 used herein is 68% conserved within the DOCK A GEFs (48); thus, we predict that RAC2^{E62K} can be activated by other DOCK A GEFs as well. Because DOCK GEFs are only catalytically active with RAC and CDC42 GTPases, this mutant in the context of RAS or RHOA likely lacks a similar compensatory mechanism for activation.

Based on our RAC2^{E62K} results and the previous study of KRAS^{E62K} GEF activity (14), we predict that the E62K mutation in the context of RAC1 and RHOA GTPases will not significantly perturb GTPase structure or nucleotide binding but will

be defective in DH-GEF–stimulated nucleotide exchange (16–19). However, RHOA and RAS GTPases differ from RAC GTPases in that they are not activated by DOCK GEFs. Retention of DOCK GEF regulation may partly compensate for the loss in DH-GEF activity. As RAC1 and RAC2 are >90% homologous, with the most significant differences restricted to the hypervariable C terminus (60), we anticipate that $RAC1^{E62K}$ will possess structure and effector recognition similar to that of $RAC2^{E62K}$.

Whereas $RAC2^{E62K}$ alters regulation by GEFs and GAPs, binding is retained with at least two downstream effectors, the $p67^{phox}$ subunit of NOX2 and PAK (Fig. 6). These results are consistent with the known binding interfaces of the $p67^{phox}$ and PAK-RBDs with RAC (Fig. 6*A*). The PAK-RBD binds RAC and CDC42 GTPases via β2 and switch II (55, 61), whereas the tricopeptide repeat (TPR) domain, also known as the RBD, of $p67^{phox}$ binds the β5/α5 loop and switch I (51). Our finding that $RAC2^{E62K}$ retains binding to $p67^{phox}$ and PAK-RBDs (Fig. 6) suggests that the E62K mutation does not induce significant structural changes in switch I, switch II, or β1–3 in the activated GTP-bound state of $RAC2^{E62K}$ and is consistent with our structural analyses. We predict that the E62K mutation will only perturb binding to those effectors that directly bind or change the orientation of Glu^{62}. However, based on our review of RAC effector complexes, no effectors that bind Glu^{62} have been identified, and we do not predict that $RAC2^{E62K}$ will perturb interactions with these known effectors (61).

Our findings of enhanced $RAC2^{E62K}$ activation in COS cells (2) and retention of $RAC2^{E62K}$ $p67^{phox}$–RBD binding are consistent with the increased and sustained superoxide production in $RAC2^{E62K/+}$ neutrophils and COS cells (2). RAC2 activation and RAC2-$p67^{phox}$ binding are the final steps toward NOX activation and superoxide production (50). Whereas the association of RAC2 with $p67^{phox}$ has a single function, the association of activated RAC with PAK results in the phosphorylation of a myriad of PAK targets (11). In neutrophils, PAK's roles include regulating extracellular trap formation (neutrophil extracellular traps) (62), NOX2 activation (through $p47^{phox}$) (63), and cell migration (10). Whereas $RAC2^{E62K}$ neutrophils have F-actin and chemotaxis defects (2), our results indicate that these defects are not caused by a change in PAK-binding affinity. We predict that the phenotypes observed in $RAC2^{E62K}$ neutrophils are driven by $RAC2^{E62K}$ hyperactivation, caused by the GAP defect we observed previously (2). However, differences in cell signaling are likely mediated by a shift in GEF recognition. Defects in DH domain GEF-mediated activation will likely shift the stimuli that activate RAC2 toward those that activate DOCK GEFs. A loss in DH domain GEF activity, and likely binding, would alter which effectors $RAC2^{E62K}$ colocalizes with, given the additional function of GEFs as scaffolding proteins (20, 21, 43). Multiple studies are needed to understand the roles of RAC GEFs in RAC2-mediated hematopoietic cell signaling before the effects of the E62K mutation, and the resulting defects in GEF catalytic activity, can be characterized in neutrophils.

In conclusion, our results suggest that the E62K mutation dysregulates RAC2 activity by perturbing interactions with GAPs and a subset of GEFs. These perturbations by the E62K mutation are likely present in other GTPases, as Glu^{62} is highly conserved in RAS and RHO subclass GTPases. The perturbation of GAP activity by the E62K mutation is an important mode of RAC2 hyperactivation in CVID. This mutation may promote activation of other GTPases in human cancers, such as the $KRAS^{E62K}$ mutation identified in malignant melanoma (16–19). The Glu^{62} residue in RAC GTPases plays a key role in GEF-stimulated GDP dissociation for DH domain but not DOCK domain GEFs; thus, the E62K mutation likely shifts GEF recognition toward DOCK GEFs. Glutamate 62 mutations are an important mode of GTPase dysregulation that drives $RAC2^{E62K/+}$-induced CVID (2) and may drive RAS Glu^{62} mutant cancers (18, 36).

Materials and methods

Plasmids, protein expression, and purification

Genes for $RAC2^{WT}$ and $RAC2^{E62K}$ were cloned into the pQlinkH vector using primers encoding for the BamHI and NotI cut sites. A stop codon was inserted prior to the NotI cut site to truncate RAC2 prior to the C-terminal CSLL motif. The CSLL motif is geranylgeranylated in mammalian cells but remains unstructured and unmodified in bacteria, thus necessitating its removal. The bacterial expression plasmid containing the gene for His-tagged $KRAS^{E62K}$ was generated by site-directed mutagenesis from the $KRAS^{WT}$ plasmid (human KRAS 4B, 1–169, C118S) in a pET21a vector. The bacterial expression plasmid for the catalytic GAP domain of human p120 RASGAP in the pQlinkH vector was described previously (38). The gene for catalytic GEF domain of human TIAM1 (residues 1033–1406) was a gift from the Sondek laboratory at the University of North Carolina (Chapel Hill, NC, USA) (45) and cloned into pGEX2T vector using EcoRI and AatII restriction enzymes. Our laboratory has used this plasmid described previously (28). The DHR2 catalytic GEF domain of the human DOCK2 (residues 1211-1624) gene in the pLic-MBP vector was a gift of the Sondek laboratory The Rac-binding domain of human PAK2 (residues 69–132, P76L,M98L) in a pGEX 2× vector was also a gift from Keith Burridge. It contains an additional eight C-terminal (KETVNNQK) residues that are homologous to PAK3. This PAK-RBD protein construct has been verified to bind activated RAC1/2 and CDC42 with high affinity (64) and has been used extensively to pull down activated RAC and CDC42 from whole-cell lysates. The His-tagged TPR domain of $p67^{phox}$ in a pET30a+ was a gift from Edgar Pick (University of Tel Aviv). All plasmids were transfected into BL21 (DE3) codon + RIL (Agilent) and expressed at 18 °C after induction with 0.5 mM isopropyl 1-thio-β-D-galactopyranoside as described previously (2). The RAC2, p50 RHOGAP, DOCK2, p120 RASGAP, $p67^{phox}$, and FLIPPi 5U were purified using nickel nitrilotriacetic acid resin (Qiagen), followed by tobacco etch virus cleavage (for RAC2 KRAS and RASGAP) and gel filtration as described previously (28). The TIAM1 and PAK proteins were purified using GST-agarose (GE Healthcare) followed by thrombin cleavage and gel filtration as described (28).

The pRSet Flippi 5U plasmid, for use in the GTP hydrolysis assays, was obtained from Addgene (37) and transformed into

BL21 DE3 codon + RIL. The transformed cells were grown in lysogeny broth supplemented with 33 mg/liter chloramphenicol and 100 mg/liter ampicillin at 21 °C for 60 h in the dark. Prior to harvesting, phosphate-free buffers were prepared using nucleoside phosphorylase and inosine as described (65). All buffers containing inosine were rendered phosphate-free by dialyzing against 5 units of nucleoside phosphorylase for 48 h at room temperature. The cells were harvested via centrifugation and resuspended in phosphate-free lysis buffer (20 mM Tris (pH 7.9), 50 mM NaCl, 20 mM imidazole, 1 mM inosine, 1 mg/ml phenylmethylsulfonyl fluoride, 0.2 μl/ml protease inhibitor mixture (Sigma, P8849)) and then lysed via sonication. Cell debris was pelleted by centrifuging for 45 min at 15,000 × *g* at 4 °C. His-tagged FLIPPI 5U was purified in lysis buffer on nickel-nitrilotriacetic acid–agarose resin as described (64). Purification was completed on a 25-ml Q-column using a 15-column volume gradient of 20–80% high-salt buffer (20 mM Tris (pH 7.9), 500 mM NaCl, 1 mM inosine, 200 mM imidazole, 5 mM β-mercaptoethanol). Purity was verified at >95% via SDS-PAGE, and the protein was stored at −80 °C until use.

GMPPCP nucleotide loading and HPLC analysis

The recombinant RAC2 GTPases were loaded with the nonhydrolyzable GTP analog GMPPCP for CD and isothermal titration calorimetry experiments as described previously (28). The protein was buffer-exchanged into nucleotide-loading buffer (20 mM Hepes (pH 8.0), 125 mM $(NH_4)_2SO_4$, 1 mM EDTA, 50 mM NaCl, 1 mM DTT) to remove excess $MgCl_2$ and GDP. Approximately 600 μl of 100 μM RAC2 was incubated with 1 mM $MgCl_2$ and 500 μM GMPPCP overnight at 4 °C in the presence of 3 units of calf intestine alkaline phosphatase–agarose (AP beads). The AP beads were removed by centrifugation. Nucleotide binding was induced by the addition of excess 10 mM $MgCl_2$. To verify the hydrolysis of GDP (by alkaline phosphatase), an aliquot of protein and nucleotide standards, GDP and GMPPCP, were boiled and centrifuged, and the supernatant was analyzed via HPLC. The nucleotide standards and samples were individually injected onto a Zorbax C-18 column in an HPLC system (Agilent 1100 series) that was pre-equilibrated with 100 mM potassium phosphate (pH 6.5), 10 mM tetrabutylammonium bromide, and 5% acetonitrile. The nucleotides were eluted using an isocratic elution at 0.5 ml/min over 20 min. The elution times were used to verify >90% GMPPCP loading.

CD and thermal stability assays

CD experiments were performed in triplicate as described previously (28). Prior to CD measurements, recombinant RAC2 protein was buffer exchanged in CD buffer (10 mM KH_2PO_4/K_2HPO_4 (pH 6.5), 500 μM $MgCl_2$, 15 μM GDP (or GMPPCP)) and concentrated to 5 μM. Constant and variable temperature CD measurements were conducted using a Jasco J-815 instrument equipped with a temperature control system (Jasco PTC-423S) and a water bath (Fisher Isotemp 3016S). Constant temperature CD scans were performed at 20 °C using a 1-mm path length over 200 to 250 nm. Each scan is the average of three individual scans (accumulations). The Jasco wavelength scan settings used were: 2-s digital integration time, 2-nm bandwidth, and 10-nm/min scanning speed. All data are reported in units of mean residue ellipticity, which was calculated as follows, $\theta_{MRE} = (\theta_{raw} \times MRW)/(10 \times c \times l)$, where θ_{raw} is the ellipticity in degrees, MRW (mean residue weight) is (molecular mass (in Da)/(number of residues) − 1), c is the concentration in g/ml, and l is the path length in cm. Immediately after the constant-temperature buffer and protein scans, thermal melts were completed by monitoring the CD signal at 222 nm while increasing the temperature 1.5 °C/min from 20 to 95 °C using a 16-s digital integration time and 1-nm bandwidth. The thermal melting temperature or unfolding temperature was calculated by plotting the change in mean residue ellipticity with temperature and fitting it to a Boltzmann sigmoidal curve using GraphPad Prism.

Molecular dynamics simulations

Molecular dynamics simulations were completed for each of the four RAC2 configurations ($RAC2^{WT}$ and $RAC2^{E62K}$, each in the GDP- and GTP-bound conformations). Models were generated for the simulations from existing crystal structures. The GDP-bound $RAC2^{WT}$ model was generated from the 1.95 Å crystal structure of $RAC2^{G12V}$ in complex with GDP (PDB entry 2W2T) (26). Prior to the molecular dynamics simulations, the RAC2 Val^{12} mutant was substituted with the Gly^{12} residue in PyMOL (PyMOL Molecular Graphics System, version 1.2r3pre, Schrödinger, LLC).

Given the high sequence homology (>90%) between RAC1 and RAC2, we generated the starting structure of GTP-bound $RAC2^{WT}$ from the existing structure of $RAC1^{WT}$ bound to the nonhydrolyzable GTP analog, GMPPNP. The 1.38 Å crystal structure of human RAC1 (PDB entry 1MH1) (22) was mutated at 9 amino acid positions to the human RAC2 sequence using PyMOL. Residues mutated included G48S, S78F, F90Y, Y98F, N107S, T135A, M145L, G150D, and A151S. All substitutions were tolerated as suitable rotamers were selected that avoided steric clashes. Further, the N3B atom in the GTP analog GMPPNP was converted to O3B. These modifications generated a model of human RAC2 in the GTP-bound conformation for the running of molecular dynamics simulations.

Three replicate molecular dynamics (MD) simulations were completed for each of the four configurations (RAC2 and E62K-RAC2 for both GDP- and GTP-bound conformations) for a total of 12 simulations. The CUDA version of PMEMD (66–68) from the Amber18 suite of programs (University of California, San Francisco) (69) was used for conducting the simulations. Protein parameters were from the ff14SB force field (70), and nucleotide parameters were from the Bryce Group Computation Biophysics and Drug Design Amber parameter database (RRID:SCR_018815) (71). Starting structures were placed in an octagonal box containing TIP3P waters that extended at least 16.0 Å from the protein surface. Counter ions were included to bring the charge of the system to zero. While the system was neutralized and the cofactor Mg^{2+} was present, no additional ions were added, giving an unphysiologically low aqueous medium, which leads to an overemphasis of electrostatic interactions in the simulations. Parameter and topology

files were generated using the tleap program (71). The SHAKE algorithm was applied for constraining bonds involving hydrogens. The particle-mesh Ewald method was used for electrostatic interaction calculations with a cutoff of 8 Å. Production runs were under constant volume and constant temperature periodic boundary conditions with an Andersen thermostat. For minimization, 5000 steps of steepest descent were followed by 5000 steps of conjugate gradient. The system was then heated from 0 to 300 K over a period of 500 ps of constant volume dynamics. Density was then equilibrated with 500 ps of constant pressure dynamics before production runs were started.

Each production simulation ran for a total length of 750 ns with a 2-fs time step, recording snapshots every 10 ps. The analysis was conducted using the CPPTRAJ program included in the AMBER suite of programs (72). The first 100 ns of the snapshots was designated as the equilibration time and excluded from further analyses. Clusters were identified in the combined trajectories from the three replicates using the density peaks (dpeaks) algorithm (30). Appropriate cutoffs for distance and density for each of the four complexes were chosen based on visual inspection of the density *versus* minimum distance plot. Density and distance cutoffs were chosen to select the outliers as putative cluster centers.

GTP hydrolysis assays

Intrinsic and GAP-stimulated GTP hydrolysis rates were determined for KRAS by measuring the production of phosphate using the phosphate-binding protein, Flippi 5U, as described previously (38, 65). All buffers were made phosphate-free using nucleoside phosphorylase as described above for preparing Flippi 5U. To remove excess GDP, $MgCl_2$, and P_i, the KRAS protein was exchanged into a chelating buffer containing 20 mM Hepes (pH 8.0), 125 mM $(NH_4)_2SO_4$, 1 mM EDTA, 2 mM inosine, 50 mM NaCl. Next, KRAS, FLIPPi 5U, and p120 RASGAP were exchanged into the hydrolysis reaction buffer, which contained 20 mM Hepes (pH 7.4), 50 mM NaCl, 2 mM inosine. Just prior to the reaction, 1 mM GTP was incubated 100 μM KRAS at 37 °C for 2 min. Unbound GTP was removed using a Zeba spin desalting column (Thermo). Hydrolysis was initiated by the addition of 20 μM $MgCl_2$ to a 384-well plate containing 5 μM KRAS and 5 μM Flippi 5U (with and without p120 RASGAP). For GAP-stimulated GTP hydrolysis, half of the wells also contained 25 nM p120 RASGAP (200:1 RAC2/GAP). Production of phosphate was measured by monitoring the Flippi FRET signal (excitation, 435 nm; emission ratio for 530 and 485 nm, 475-nm cutoff) using a SpectraMax M5 microplate reader. The data were normalized and fit to a single-phase exponential using GraphPad Prism. GTP hydrolysis rates were calculated using a single-phase association in GraphPad Prism and are representative of two independent experiments. Significance was calculated using one-way analysis of variance followed by Tukey's multiple-comparison test in GraphPad Prism.

GDP dissociation assays

Intrinsic and GEF-stimulated GDP dissociation rates were determined by observing the dissociation of MANT-GDP (Jena) over time in the absence and presence of TIAM1 or DOCK2. First, RAC2 was buffer-exchanged into a low-Mg buffer (20 mM Hepes (pH 8.0), 125 mM $(NH_4)_2SO_4$, 0.1 mM EDTA) to remove excess GDP and $MgCl_2$. MANT-GDP loading was achieved by incubating 10 μM RAC2 in 100 μM MANT-GDP for 40 min at 37 °C followed by the addition of 20 mM $MgCl_2$ and 1-h incubation at 4 °C. Excess MANT-GDP was removed by buffer exchange into 20 mM Hepes (pH 7.4), 50 mM NaCl, 5 mM $MgCl_2$, and 100 μM DTPA. Nucleotide dissociation was initiated by adding 1000-fold excess unlabeled GDP. MANT-GDP dissociation was measured using fluorescence emission at 435 nm (excitation, 365 nm) on a SpectraMax M5 microplate reader. The nucleotide dissociation rates (k_{obs}) at each concentration of GEF were calculated by fitting the fluorescence signal to a one-phase exponential decay equation using GraphPad Prism. k_{obs} values are representative of three independent experiments and are plotted as the mean ± S.D. The change in the RAC2 GDP dissociation rate was plotted as a function of GEF concentration (0 μM (intrinsic), 0.3, 0.6, 1, 1.5, 2, 3, 4.5, 7, and 10 μM) and was then fit to the k_{cat} function in GraphPad Prism to calculate catalytic activity (k_{cat}). k_{cat} is reported as the mean ± S.E., and significance was determined using an unpaired *t* test.

Isothermal titration calorimetry binding assays

The RAC2-binding affinity for PAK and $p67^{phox}$ were measured using ITC. GMPPCP-preloaded RAC2 and effector proteins, $p67^{phox}$ and PAK-RBD, were exchanged into ITC buffer (20 mM Hepes (pH 7.4), 50 mM NaCl, 5 mM $MgCl_2$, 1 mM tris(2-carboxyethyl)phosphine). ITC experiments were conducted using a MicroCal autoITC200 instrument at the University of North Carolina Macromolecular Interactions Facility within the Center for Structural Biology. All ITC experiments were completed at 25 °C using the same ITC settings. $RAC2^{WT}$ and $RAC2^{E62K}$ samples were run in sequence for each experimental replicate. The heat released or required during binding was measured for 20 2-μl injections of the effector protein (either PAK-RBD or $p67^{phox}$) into the sample cell containing RAC2. The baseline heat for each experiment was set to 7, and the injections were added 180 s apart to allow a complete return to the baseline heat prior to the next injection. Origin software was used to calculate the binding affinity, stoichiometry, enthalpy, and entropy. GraphPad Prism was used to calculate the mean and S.D. for the replicate experiments (n = 2 for PAK, n = 3 for $p67^{phox}$).

Data availability

All data are included within the article and supporting information.

Acknowledgments—We thank Brian Kuhlman (UNC Department of Biochemistry and Biophysics) and Ashutosh Tripathy (UNC Macromolecular Interactions Facility) for the training in and use of the circular dichroism and isothermal titration calorimetry instruments, respectively.

Author contributions—M. E. A., B. T., A. S., and S. L. C. conceptualization; M. E. A. and B. T. data curation; M. E. A. and

B. T. formal analysis; M. E. A. validation; M. E. A. and S. L. C. investigation; M. E. A. and B. T. visualization; M. E. A., B. T., and A. S. methodology; M. E. A., B. T., and S. L. C. writing-original draft; M. E. A., B. T., A. S., and S. L. C. writing-review and editing; B. T. resources; B. T. software; S. L. C. supervision; S. L. C. funding acquisition; S. L. C. project administration.

Funding and additional information—This work was supported by NCI, National Institutes of Health, Grants P01 CA203657 (to S. L. C), R01 CA224428 (to A. S.), and P30 CA016086 (to the UNC Center of Structural Biology). The content is solely the responsibility of the authors and does not necessarily reflect the official views of the National Institutes of Health.

Conflict of interest—The authors declare that they have no conflicts of interest with the contents of this article.

Abbreviations—The abbreviations used are: RAC, RAS-related C3 botulinum toxin substrate; AMBER, assisted model building with energy refinement program; AP, alkaline phosphatase; CDC42, cell division control protein 42 homolog; CVID, common variable immune deficiency; DH, Dbl homology; DHR2, DOCK homology region 2; DOCK, dedicator of cytokinesis; FLIPPi, fluorescent indicator protein for inorganic phosphate; GAP, GTPase-activating protein; GDI, guanine nucleotide dissociation inhibitor; GEF, guanine nucleotide exchange factor; GMPPCP, β,γ-methyleneguanosine 5′-triphosphate; GMPPNP, 5′-guanylyl imidodiphosphate; ITC, isothermal titration calorimetry; MANT, 2′-/3′-*O*-(*N*′-methylanthraniloyl); MD, molecular dynamics; NOX, NADPH oxidase; PAK, p21-activated kinase; PDB, Protein Data Bank; PREX1, phosphatidylinositol 3,4,5-triphosphate–dependent Rac exchange factor; RBD, Rac-binding domain; RHOA, RAS homolog family member A; RMSD, root mean square deviation; SOS, son of sevenless; TIAM1, T-cell lymphoma invasion and metastasis-inducing protein-1; T_m, thermal melting temperature; TPR, tetratricopeptide repeat motif.

References

1. Gu, Y., Filippi, M.-D., Cancelas, J. A., Siefring, J. E., Williams, E. P., Jasti, A. C., Harris, C. E., Lee, A. W., Prabhakar, R., Atkinson, S. J., Kwiatkowski, D. J., and Williams, D. A. (2003) Hematopoietic cell regulation by Rac1 and Rac2 guanosine triphosphatases. *Science* **302,** 445–449 CrossRef Medline
2. Hsu, A. P., Donkó, A., Arrington, M. E., Swamydas, M., Fink, D., Das, A., Escobedo, O., Bonagura, V., Szabolcs, P., Steinberg, H. N., Bergerson, J., Skoskiewicz, A., Makhija, M., Davis, J., Foruraghi, L., *et al.* (2019) Dominant activating RAC2 mutation with lymphopenia, immunodeficiency and cytoskeletal defects. *Blood* **133,** 1977–1988 CrossRef Medline
3. Vetter, I. R., and Wittinghofer, A. (2001) The guanine nucleotide-binding switch in three dimensions. *Science* **294,** 1299–1304 CrossRef Medline
4. Watanabe, M., Terasawa, M., Miyano, K., Yanagihara, T., Uruno, T., Sanematsu, F., Nishikimi, A., Côté, J.-F., Sumimoto, H., and Fukui, Y. (2014) DOCK2 and DOCK5 act additively in neutrophils to regulate chemotaxis, superoxide production, and extracellular trap formation. *J. Immunol.* **193,** 5660–5667 CrossRef Medline
5. Mulloy, J. C., Cancelas, J. A., Filippi, M.-D., Kalfa, T. A., Guo, F., and Zheng, Y. (2010) Rho GTPases in hematopoiesis and hemopathies. *Blood* **115,** 936–947 CrossRef Medline
6. Ambruso, D. R., Knall, C., Abell, A. N., Panepinto, J., Kurkchubasche, A., Thurman, G., Gonzalez-Aller, C., Hiester, A., deBoer, M., Harbeck, R. J., Oyer, R., Johnson, G. L., and Roos, D. (2000) Human neutrophil immunodeficiency syndrome is associated with an inhibitory Rac2 mutation. *Proc. Natl. Acad. Sci. U. S. A.* **97,** 4654–4659 CrossRef Medline
7. Hodge, R. G., and Ridley, A. J. (2016) Regulating Rho GTPases and their regulators. *Nat. Rev. Mol. Cell Biol.* **17,** 496–510 CrossRef Medline
8. Cook, D. R., Rossman, K. L., and Der, C. J. (2014) Rho guanine nucleotide exchange factors: regulators of Rho GTPase activity in development and disease. *Oncogene* **33,** 4021–4035 CrossRef Medline
9. Thomas, D. C. (2017) The phagocyte respiratory burst: historical perspectives and recent advances. *Immunol. Lett.* **192,** 88–96 CrossRef Medline
10. Itakura, A., Aslan, J. E., Kusanto, B. T., Phillips, K. G., Porter, J. E., Newton, P. K., Nan, X., Insall, R. H., Chernoff, J., and McCarty, O. J. T. (2013) p21-activated kinase (PAK) regulates cytoskeletal reorganization and directional migration in human neutrophils. *PLoS ONE* **8,** e73063 CrossRef Medline
11. Kumar, R., Sanawar, R., Li, X., and Li, F. (2017) Structure, biochemistry, and biology of PAK kinases. *Gene* **605,** 20–31 CrossRef Medline
12. Wittinghofer, A., and Vetter, I. R. (2011) Structure-function relationships of the G domain, a canonical switch motif. *Annu. Rev. Biochem.* **80,** 943–971 CrossRef Medline
13. Krauthammer, M., Kong, Y., Ha, B. H., Evans, P., Bacchiocchi, A., McCusker, J., Cheng, E., Davis, M. J., Goh, G., Choi, M., Holman, E. C., Bosenberg, M., Sznol, M., Kluger, H. M., Brash, D. E., *et al.* (2012) Exome sequencing identifies recurrent somatic Rac1 mutations in melanoma. *Nat. Genet.* **44,** 1006–1014 CrossRef Medline
14. Gasper, R., Thomas, C., Reza Ahmadian, M., and Wittinghofer, A. (2008) The role of the conserved switch II glutamate in guanine nucleotide exchange factor-mediated nucleotide exchange of GTP-binding proteins. *J. Mol. Biol.* **379,** 51–63 CrossRef Medline
15. Bos, J., Rehmann, H., and Wittinghofer, A. (2007) GEFs and GAPs : critical elements in the control of small G proteins. *Cell* **129,** 865–877 CrossRef
16. Kim, E., Ilic, N., Shrestha, Y., Zou, L., Kamburov, A., Zhu, C., Yang, X., Lubonja, R., Tran, N., Nguyen, C., Lawrence, M. S., Piccioni, F., Bagul, M., Doench, J. G., Chouinard, C. R., *et al.* (2016) Systematic functional interrogation of rare cancer variants identifies oncogenic alleles. *Cancer Discov.* **6,** 714–726 CrossRef Medline
17. Zehir, A., Benayed, R., Shah, R. H., Syed, A., Middha, S., Kim, H. R., Srinivasan, P., Gao, J., Chakravarty, D., Devlin, S. M., Hellmann, M. D., Barron, D. A., Schram, A. M., Hameed, M., Dogan, S., *et al.* (2017) Mutational landscape of metastatic cancer revealed from prospective clinical sequencing of 10,000 patients. *Nat. Med.* **23,** 703–713 CrossRef Medline
18. Tate, J. G., Bamford, S., Jubb, H. C., Sondka, Z., Beare, D. M., Bindal, N., Boutselakis, H., Cole, C. G., Creatore, C., Dawson, E., Fish, P., Harsha, B., Hathaway, C., Jupe, S. C., Kok, C. Y., *et al.* (2019) COSMIC: the catalogue of somatic mutations in cancer. *Nucleic Acids Res.* **47,** D941–D947 CrossRef Medline
19. Dika, E., Altimari, A., Patrizi, A., Gruppioni, E., Fiorentino, M., Piraccini, B. M., Misciali, C., Barisani, A., and Fanti, P. A. (2013) KIT, NRAS, and BRAF mutations in nail apparatus melanoma. *Pigment Cell Melanoma Res.* **26,** 758–760 CrossRef Medline
20. Marei, H., and Malliri, A. (2017) GEFs: dual regulation of Rac1 signaling. *Small GTPases* **8,** 90–99 CrossRef Medline
21. Lawson, C. D., and Ridley, A. J. (2018) Rho GTPase signaling complexes in cell migration and invasion. *J. Cell Biol.* **217,** 447–457 CrossRef Medline
22. Pan, D., Wakelam, M. J., Welch, H. C. E., Amison, R. T., Riffo-Vasquez, Y., Spina, D., Cleary, S. J., Page, C. P., and Pitchford, S. C. (2015) P-Rex and Vav Rac-GEFs in platelets control leukocyte recruitment to sites of inflammation. *Blood* **125,** 1146–1158 CrossRef Medline
23. Hirshberg, M., Stockley, R. W., Dodson, G., and Webb, M. R. (1997) The Crystal Structure of human Rac1, a member of the rho-family complexed with a GTP analogue. *Nat. Struct. Biol.* **4,** 147–152 CrossRef Medline
24. Ferrandez, Y., Zhang, W., Peurois, F., Akendengué, L., Blangy, A., Zeghouf, M., and Cherfils, J. (2017) Allosteric inhibition of the guanine nucleotide exchange factor DOCK5 by a small molecule. *Sci. Rep.* **7,** 14409 CrossRef
25. Davis, M. J., Hak, B., Holman, E. C., Halaban, R., Schlessinger, J., Boggon, T. J., and Ha, B. H. (2013) RAC1P29S is a spontaneously activating cancer-associated GTPase. *Proc. Natl. Acad. Sci. U. S. A.* **110,** 912–917 CrossRef Medline
26. Bunney, T. D., Opaleye, O., Roe, S. M., Vatter, P., Baxendale, R. W., Walliser, C., Everett, K. L., Josephs, M. B., Christow, C., Rodrigues-Lima, F., Gierschik, P., Pearl, L. H., and Katan, M. (2009) Structural insights into

formation of an active signaling complex between Rac and phospholipase C γ2. *Mol. Cell.* **34,** 223–233 CrossRef Medline
27. Kelly, S. M., Jess, T. J., and Price, N. C. (2005) How to study proteins by circular dichroism. *Biochim. Biophys. Acta* **1751,** 119–139 CrossRef Medline
28. Hobbs, G. A., Mitchell, L. E., Arrington, M. E., Gunawardena, H. P., Decristo, M. J., Loeser, R. F., Chen, X., Cox, A. D., and Campbell, S. L. (2015) Redox regulation of Rac1 by thiol oxidation. *Free Radic. Biol. Med.* **79,** 237–250 CrossRef Medline
29. Yin, G., Kistler, S., George, S. D., Kuhlmann, N., Garvey, L., Huynh, M., Bagni, R. K., Lammers, M., Der, C. J., and Campbell, S. L. (2017) A KRAS GTPase K104Q mutant retains downstream signaling by offsetting defects in regulation. *J. Biol. Chem.* **292,** 4446–4456 CrossRef Medline
30. Rodriguez, A., and Laio, A. (2014) Clustering by fast search and find of density peaks. *Science* **344,** 1492–1496 CrossRef Medline
31. Haeusler, L. C., Blumenstein, L., Stege, P., Dvorsky, R., and Ahmadian, M. R. (2003) Comparative functional analysis of the Rac GTPases. *FEBS Lett.* **555,** 556–560 CrossRef Medline
32. Graham, D. L., Lowe, P. N., Grime, G. W., Marsh, M., Rittinger, K., Smerdon, S. J., Gamblin, S. J., and Eccleston, J. F. (2002) MgF_3^- as a transition state analog of phosphoryl transfer. *Chem. Biol.* **9,** 375–381 CrossRef Medline
33. Rittinger, K., Walker, P. A., Eccleston, J. F., Nurmahomed, K., Owen, D., Laue, E., Gamblin, S. J., and Smerdon, S. J. (1997) Crystal structure of a small G protein in complex with the GTPase-activating protein rhoGAP. *Nature* **388,** 693–697 CrossRef Medline
34. Scheffzek, K., Ahmadian, M. R., Kabsch, W., Wiesmüller, L., Lautwein, A., Schmitz, F., Wittinghofer, A., Wiesmöller, L., and Wittinghofer, A. (1997) The Ras-RasGAP complex: structural basis for GTPase activation and its loss in oncogenic Ras mutants. *Science* **277,** 333–338 CrossRef Medline
35. Würtele, M., Wolf, E., Pederson, K. J., Buchwald, G., Ahmadian, M. R., Barbieri, J. T., and Wittinghofer, A. (2001) How the *Pseudomonas aeruginosa* ExoS toxin downregulates Rac. *Nat. Struct. Biol.* **8,** 23–26 CrossRef Medline
36. Murugan, A. K., Hong, N. T., Cuc, T. T. K., Hung, N. C., Munirajan, A. K., Ikeda, M. A., and Tsuchida, N. (2009) Detection of two novel mutations and relatively high incidence of H-RAS mutations in Vietnamese oral cancer. *Oral. Oncol.* **45,** e161–e166 CrossRef Medline
37. Gu, H., Lalonde, S., Okumoto, S., Looger, L. L., Scharff-Poulsen, A. M., Grossman, A. R., Kossmann, J., Jakobsen, I., and Frommer, W. B. (2006) A novel analytical method for *in vivo* phosphate tracking. *FEBS Lett.* **580,** 5885–5893 CrossRef Medline
38. Baker, R. A., Lewis, S. M., Sasaki, A. T., Wilkerson, E. M., Locasale, J. W., Cantley, L. C., Kuhlman, B., Dohlman, H. G., and Campbell, S. L. (2013) Site-specific monoubiquination activates Ras by impeding GTPase activating protein function. *Nat. Struct. Mol. Biol.* **20,** 46–52 CrossRef Medline
39. Hobbs, G. A., Bonini, M. G., Gunawardena, H. P., Chen, X., and Campbell, S. L. (2013) Glutathiolated Ras: characterization and implications for Ras activation. *Free Radic. Biol. Med.* **57,** 221–229 CrossRef Medline
40. Worthylake, D. K., Rossman, K. L., and Sondek, J. (2000) Crystal structure of Rac1 in complex with the guanine nucleotide exchange region of Tiam1. *Nature* **408,** 682–688 CrossRef Medline
41. Boriack-Sjodin, P. A., Margarit, S. M., Bar-Sagi, D., and Kuriyan, J. (1998) The structural basis of the activation of Ras by Sos. *Nature* **394,** 337–343 CrossRef Medline
42. Snyder, J. T., Worthylake, D. K., Rossman, K. L., Betts, L., Pruitt, W. M., Siderovski, D. P., Der, C. J., and Sondek, J. (2002) Structural basis for the selective activation of Rho GTPases by Dbl exchange factors. *Nat. Struct. Biol.* **9,** 468–475 CrossRef Medline
43. Pantarelli, W. (2018) Rac-GTPases and Rac-GEFs in neutrophil adhesion, migration and recruitment. *Eur. J. Clin. Invest.* **48,** e12939 CrossRef Medline
44. McCormick, B., Chu, J. Y., and Vermeren, S. (2019) Cross-talk between Rho GTPases and PI3K in the neutrophil. *Small GTPases* **10,** 187–195 CrossRef Medline
45. Karnoub, A. E., Worthylake, D. K., Rossman, K. L., Pruitt, W. M., Campbell, S. L., Sondek, J., and Der, C. J. (2001) Molecular basis for Rac1 recognition by guanine nucleotide exchange factors. *Nat. Struct. Biol.* **8,** 1037–1041 CrossRef Medline
46. Chrencik, J. E., Broun, A., Zhang, H., Mathews, I. I., Hura, G. L., Foster, S. A., Perry, J. J. P., Streiff, M., Ramage, P., Widmer, H., Bokoch, G. M., Tainer, J. A., Weckbecker, G., and Kuhn, P. (2008) Structural basis of guanine nucleotide exchange mediated by the T-cell essential Vav1. *J. Mol. Biol.* **380,** 828–843 CrossRef Medline
47. Lucato, C. M., Halls, M. L., Ooms, L. M., Liu, H. J., Mitchell, C. A., Whisstock, J. C., and Ellisdon, A. M. (2015) The phosphatidylinositol (3,4,5)-trisphosphate-dependent Rac exchanger 1·Ras-related C3 botulinum toxin substrate 1 (P-Rex1·Rac1) complex reveals the basis of Rac1 activation in breast cancer cells. *J. Biol. Chem.* **290,** 20827–20840 CrossRef Medline
48. Cote, J.-F. (2002) Identification of an evolutionarily conserved superfamily of DOCK180-related proteins with guanine nucleotide exchange activity. *J. Cell Sci.* **115,** 4901–4913 CrossRef
49. Kulkarni, K., Yang, J., Zhang, Z., and Barford, D. (2011) Multiple factors confer specific Cdc42 and Rac protein activation by dedicator of cytokinesis (DOCK) nucleotide exchange factors. *J. Biol. Chem.* **286,** 25341–25351 CrossRef Medline
50. Pick, E. (2014) Role of the Rho GTPase Rac in the activation of the phagocyte NADPH oxidase. *Small GTPases* **5,** e27952 CrossRef Medline
51. Lapouge, K., Smith, S. J. M., Walker, P. A., Gamblin, S. J., Smerdon, S. J., and Rittinger, K. (2000) Structure of the TPR domain of p67(phox) in complex with Rac·GTP. *Mol. Cell.* **6,** 899–907 CrossRef Medline
52. Bokoch, G. M., Edwards, D. C., Sanders, L. C., and Gill, G. N. (1999) Activation of LIM-kinase by Pak1 couples Rac/Cdc42 GTPase signalling to actin cytoskeletal dynamics. *Nat. Cell Biol.* **1,** 253–259 CrossRef Medline
53. Chang, L. C., Lin, R. H., Huang, L. J., Chang, C., Sen, Kuo, S. C., and Wang, J. P. (2009) Inhibition of superoxide anion generation by CHS-111 via blockade of the p21-activated kinase, protein kinase B/Akt and protein kinase C signaling pathways in rat neutrophils. *Eur. J. Pharmacol.* **615,** 207–217 CrossRef Medline
54. Arai, A., Jin, A., Yan, W., Mizuchi, D., Yamamoto, K., Nanki, T., and Miura, O. (2005) SDF-1 synergistically enhances IL-3-induced activation of the Raf-1/MEK/Erk signaling pathway through activation of Rac and its effector Pak kinases to promote hematopoiesis and chemotaxis. *Cell. Signal.* **17,** 497–506 CrossRef Medline
55. Morreale, A., Venkatesan, M., Mott, H. R., Owen, D., Nietlispach, D., Lowe, P. N., and Laue, E. D. (2000) Structure of Cdc42 bound to the GTPase binding domain of PAK. *Nat. Struct. Biol.* **7,** 384–388 CrossRef Medline
56. Yang, F.-C., Atkinson, S. J., Gu, Y., Borneo, J. B., Roberts, A. W., Zheng, Y., Pennington, J., and Williams, D. A. (2001) Rac and Cdc42 GTPases control hematopoietic stem cell shape, adhesion, migration, and mobilization. *Proc. Natl. Acad. Sci. U. S. A.* **98,** 5614–5618 CrossRef Medline
57. Cancelas, J. A., Lee, A. W., Prabhakar, R., Stringer, K. F., Zheng, Y., and Williams, D. A. (2005) Rac GTPases differentially integrate signals regulating hematopoietic stem cell localization. *Nat. Med.* **11,** 886–891 CrossRef Medline
58. Nassar, N., Hoffman, G. R., Manor, D., Clardy, J. C., and Cerione, R. A. (1998) Structures of Cdc42 bound to the active and catalytically compromised forms of Cdc42GAP. *Nat. Struct. Biol.* **5,** 1047–1052 CrossRef Medline
59. Yang, J., Zhang, Z., Roe, S. M., Marshall, C. J., and Barford, D. (2009) Activation of Rho GTPases by DOCK exchange factors is mediated by a nucleotide sensor. *Science* **325,** 1398–1403 CrossRef Medline
60. Lam, B., and Hordijk, P. (2013) The Rac1 hypervariable region in targeting and signaling: a tail of many stories. *Small GTPases* **4,** 78–89 CrossRef Medline
61. Mott, H. R., and Owen, D. (2015) Structures of Ras superfamily effector complexes: what have we learnt in two decades? *Crit. Rev. Biochem. Mol. Biol.* **50,** 85–133 CrossRef Medline
62. Gavillet, M., Martinod, K., Renella, R., Wagner, D. D., and Williams, D. A. (2018) A key role for Rac and Pak signaling in neutrophil extracellular

traps (NETs) formation defines a new potential therapeutic target. *Am. J. Hematol.* **93,** 269–276 CrossRef Medline
63. Martyn, K. D., Kim, M. J., Quinn, M. T., Dinauer, M. C., and Knaus, U. G. (2005) p21-activated kinase (Pak) regulates NADPH oxidase activation in human neutrophils. *Blood* **106,** 3962–3969 CrossRef Medline
64. Wittchen, E. S., and Burridge, K. (2008) Chapter 14 Analysis of Low Molecular Weight GTPase Activity in endothelial cell cultures. *Methods Enzymol.* **443,** 285–298 CrossRef Medline
65. Shutes, A., and Der, C. J. (2005) Real-time *in vitro* measurement of GTP hydrolysis. *Methods* **37,** 183–189 CrossRef Medline
66. Salomon-Ferrer, R., Götz, A. W., Poole, D., Le Grand, S., and Walker, R. C. (2013) Routine microsecond molecular dynamics simulations with AMBER—Part II: particle mesh Ewald. *J. Chem. Theory Comput.* **9,** 3878–3888 CrossRef Medline
67. Götz, A. W., Williamson, M. J., Xu, D., Poole, D., Le Grand, S., and Walker, R. C. (2012) Routine microsecond molecular dynamics simulations with AMBER—Part I: generalized Born. *J. Chem. Theory Comput.* **8,** 1542–1555 CrossRef Medline
68. Le Grand, S., Götz, A. W., and Walker, R. C. (2013) SPFP: Speed without compromise—a mixed precision model for GPU accelerated molecular dynamics simulations. *Comp. Phys. Commun.* **184,** 374–380 CrossRef
69. Case, D. A., Ben-Shalom, I. Y., Brozell, S. R., Cerutti, D. S., Cheatham, T. E., Cruziero, V. W. D., Darden, T. A., Duke, R. E., Ghoreishi, M. K., Gilson, M. K., Gohlke, H., Goetz, A. W., Greene, D., Harris, R., Homeyer, N., *et al.* (2018) *AMBER 2018*, University of California, San Francisco
70. Maier, J. A., Martinez, C., Kasavajhala, K., Wickstrom, L., Hauser, K. E., and Simmerling, C. (2015) ff14sB: improving the accuracy of protein side chain and backbone parameters from ff99SB. *J. Chem. Theory. Comput.* **11,** 3696–3713 CrossRef Medline
71. Meagher, K. L., Redman, L. T., and Carlson, H. A. (2003) Development of polyphosphate parameters for use with the AMBER force field. *J. Comput. Chem.* **24,** 1016–1025 CrossRef Medline
72. Case, D. A., Cheatham, T. E., Darden, T., Gohlke, H., Luo, R., Merz, K. M., Onufriev, A., Simmerling, C., Wang, B., and Woods, R. J. (2005) The Amber biomolecular simulation programs. *J. Comput. Chem.* **26,** 1668–1688 CrossRef Medline
73. Tina, K. G., Bhadra, R., and Srinivasan, N. (2007) PIC: Protein Interactions Calculator. *Nucleic Acids Res* **35,** 473–476 CrossRef Medline